Green Chemistry Letters and Reviews

ISSN: 1751-8253 (Print) 1751-7192 (Online) Journal homepage: www.tandfonline.com/journals/tgcl20

Green synthesis of silver nanoparticles using *Trema Orientalis* (L.) extract and evaluation of their antibacterial activity

Richa Das, Pradeep Kumar, Amit Kumar Singh, Shreni Agrawal, Salim Albukhaty, Indrani Bhattacharya, Kavindra Nath Tiwari, Sunil Kumar Mishra, Amit Kumar Tripathi, Faizah A. AlMalki, Azalldeen Kazal Alzubaidi, Wasan J. Al-Kaabi, Vishnu D. Rajput & Zaidon T. Al-aqbi

To cite this article: Richa Das, Pradeep Kumar, Amit Kumar Singh, Shreni Agrawal, Salim Albukhaty, Indrani Bhattacharya, Kavindra Nath Tiwari, Sunil Kumar Mishra, Amit Kumar Tripathi, Faizah A. AlMalki, Azalldeen Kazal Alzubaidi, Wasan J. Al-Kaabi, Vishnu D. Rajput & Zaidon T. Al-aqbi (2025) Green synthesis of silver nanoparticles using *Trema Orientalis* (L.) extract and evaluation of their antibacterial activity, Green Chemistry Letters and Reviews, 18:1, 2444679, DOI: 10.1080/17518253.2024.2444679

To link to this article: https://doi.org/10.1080/17518253.2024.2444679

Published online: 23 Dec 2024.

GREEN CHEMISTRY LETTERS AND REVIEWS
2025, VOL. 18, NO. 1, 2444679
https://doi.org/10.1080/17518253.2024.2444679

Taylor & Francis
Taylor & Francis Group

Green synthesis of silver nanoparticles using *Trema Orientalis* (L.) extract and evaluation of their antibacterial activity

Richa Das[a], Pradeep Kumar[b], Amit Kumar Singh[c], Shreni Agrawal[a], Salim Albukhaty[d,e], Indrani Bhattacharya[a], Kavindra Nath Tiwari[b], Sunil Kumar Mishra[c], Amit Kumar Tripathi[f], Faizah A. AlMalki[g], Azalldeen Kazal Alzubaidi[h], Wasan J. Al-Kaabi[i], Vishnu D. Rajput[j] and Zaidon T. Al-aqbi[d]

[a]Department of Biotechnology, Parul Institute of AppliedScience, Parul University, Vadodara, India; [b]Department of Botany, MMV, Banaras Hindu University, Varanasi, India; [c]Department of Pharmaceutical Engineering and Technology, Indian Institute of Technology, Banaras Hindu University, Varanasi, India; [d]Department of Chemistry, College of Science, University of Misan, Amara, Iraq; [e]Al-Manara College for Medical Sciences, Amara, Iraq; [f]School of Basic and Applied Science, Galgotias University, Noida, India; [g]Department of Biology, College of Science, Taif University, Taif, Kingdom of Saudi Arabia; [h]College of Agriculture, University of Misan, Amara, Iraq; [i]Department of Science, College of Basic Education, University of Misan, Amarah, Iraq; [j]Academy of Biology and Biotechnology, Southern Federal University, Rostov-on-Don, Russia

ABSTRACT

A novel green method was developed to create pure, safe, and stable silver nanoparticles (AgNPs) using *Trema orientalis* (L.) leaf extract as a reducing and stabilizing agent and evaluated its antibacterial activity. UV-vis spectroscopy indicated the biogenesis of AgNPs based on the absorbance in the range of 400–500 nm. The Fourier transform infrared spectroscopy (FTIR) revealed that flavonoids play a crucial role in the synthesis and stability of green AgNPs, serving as the primary phytoconstituents involved. AgNPs were spherical, and crystalline in nature. The size ranged from 14.04–34.38 nm as determined by transmission electron microscopy (TEM). For phase determination of the crystalline structure, AgNPs were subjected to X-ray diffraction (XRD). The crystallinity percentage calculated was 79.28%. The investigation using atomic force microscopy (AFM) measured the average roughness, maximum height, and valley depth of AgNPs. The mean surface roughness measured was 12.054 nm. The well diffusion method demonstrated the antibacterial activity of AgNPs against *Staphylococcus aureus*, resulting in inhibition zones measuring 9 , 10 , 13 , and 14 mm. These effects were observed at concentrations of 25 µg/mL, 50 µg/mL, 75 µg/mL, and 100 µg/mL, respectively. The minimum inhibitory concentration observed against *S. aureus* was 55.31 µg/ml. This work provides a more sustainable and efficient method of bacterial treatment.

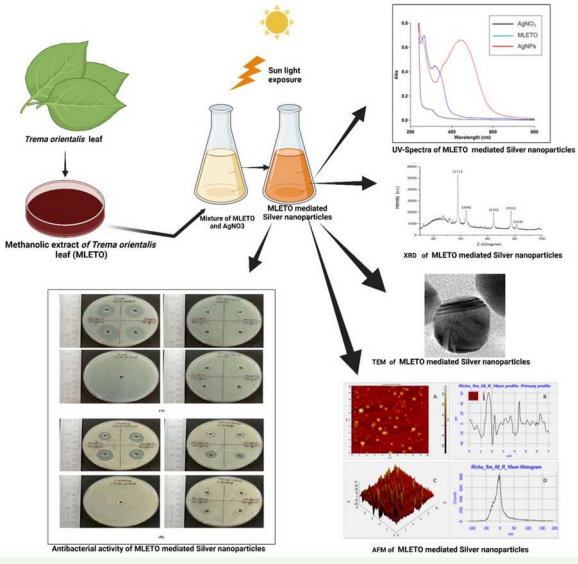

ARTICLE HISTORY

Received 10 July 2024
Accepted 13 December 2024

KEYWORDS

Silver nanoparticle; green synthesis; antimicrobial activity; *Trema orientalis* (L.)

CONTACT Salim Albukhaty albukhaty.salim@uomisan.edu.iq; Sunil Kumar Mishra skmishra.phe@itbhu.ac.in; Zaidon T. Al-aqbi zthal@utas.edu.au

1. Introduction

Nanotechnology has developed as a significant field of study (*1–4*). Nanotechnology is the technique of fabricating nanoparticles with sizes on the nanoscale, varying from 1 to 100 nm (*5*). When compared to their bulk form, nanomaterials are more versatile (*6, 7*). Due to their high surface area to volume ratio, they possess optical characteristics. These objects are of such small size that they can capture electrons and cause quantum phenomena, which in turn simplifies their detection (*8, 9*). Nanoparticles have the ability to be utilized in various fields such as sensors, optics, medicine, and engineering (*10–12*). The physiochemical qualities of metal nanoparticles, like, as high stability, and photothermal and plasmonic capabilities make them effective therapeutic agents (*13*). Since transition metals contain partially filled d-orbitals, they are more redox-active, which means, they easily get reduced to zerovalent atoms. Therefore, making transition metals is the best choice for synthesizing metal-derived nanoparticles (*14, 15*).

Silver nanoparticles (AgNPs) are popular among metal nanoparticles due to their potent antibacterial and anti-inflammation properties. AgNPs are used in a variety of biological, physical, and pharmaceutical domains. For example, AgNPs present in ointments are used to prevent bacterial infection in burns and wounds (*16*). Different techniques, like, laser ablation, sputtering, mechanical milling, liquid-state synthesis, solid-state method, and gas phase methods, are employed for the synthesis of silver nanoparticles (*17*). Nevertheless, these approaches proved to be hazardous, resulting in a desire for biologically derived nanoparticles. Plants, fungi, bacteria, and actinomycetes can be employed to biosynthesize AgNPs, eliminating the use of harmful substances and allowing for future applications in the pharmaceutical and medical fields (*18, 19*). The use of plants in the fabrication of AgNPs has received a lot of interest. The use of plant extracts for AgNP synthesis is based on the presence of high quantities of phytoconstituents, like (*20*), flavonoids, alkaloids, terpenes, saponins, and taxanes (*21*), that act as biocapping and reducing agents, therefore, decreasing the agglomeration and providing better size control of the nanoparticles (*20*). The medicinal herbs exhibit antimicrobial, anti-inflammatory, anti-aging, antiviral, and anti-cancer properties (*22*). The leaves, seeds, roots, and bark of the plants are employed in the bio-synthesis of AgNPs (*5, 23*). There are multiple examples of AgNPs being synthesized from different types of plants, such as *Carica papaya* (*24*), *Cinnamon zeylanicum* (*25*), *Datura stramonium* (*26*), *Gmelina aroberea* (*27*), *Tectona grandis* (*5*), *Carduus crispus* (*28*), and many more. Silver nanoparticles have been proposed to offer a variety of antimicrobial actions. Small-sized AgNPs produced by the plant extract with incredibly large surface area enable greater contact and interaction with the bacterial cell than bigger ones, which might explain the good antibacterial activity of AgNPs (*27*). It has been studied that when AgNPs interact with prokaryotic cells, cell division is inhibited (*28*). Silver ions produced by AgNPs may enter into cell membranes, which allows them to interact with sulfur and phosphorus-containing molecules such as DNA and proteins, therefore, inhibiting replication of DNA and eventually causing cell death (*29*). It has also been postulated that once within the bacterial cells, AgNPs can have a persistent release of silver ions (*30*), which can interact with thiol groups in enzymes like NADH dehydrogenases and impair the respiratory chain (*31*). The generation of free radicals by AgNPs causes oxidative stress, which is likely to be a second mechanism of cell death (*32*). *Trema orientalis* (L.) is a medicinal plant that belongs to the Ulmaceae family (*33*). It is found in Africa and Asia (*33*). It is often referred to as a gunpowder tree or a charcoal tree. It bears the names Gio in Hindi, Chikan or Jibon in Bengali, and Nalita in English (*30*). *T. orientalis* has pharmacological properties that include, antiplasmodial (*34*), antioxidant (*35*), antimalarial (*36*), antidiarrheal (*36*), and anti-inflammatory and antinociceptive activities (*37*).

T. orientalis stem bark extracts have been demonstrated to have antibacterial action against respiratory tract bacteria such as *Escherichia coli*, *Klebsiella pneumonia*, *Pseudomonas fluorescens*, *Proteus mirabilis*, and *Staphylococcus aureus* (*38*). Flavonoids, saponins, phenolics, tannins, triterpenes, steroids, alkaloids, and cardiac glycosides are the most abundant phytoconstituents found in *T. orientalis* (*34*). Currently, there is a lack of research on the production of AgNP using methanolic leaf extract of *T. orientalis* (MLETO). In this study, we employed a methanolic leaf extract of *T. orientalis* (MLETO) to convert silver nitrate into silver nanoparticles. The nanoparticles were then analyzed using various techniques including UV-visible spectroscopy, Fourier transform infrared spectroscopy (FTIR), transmission electron microscope (TEM), X-ray diffraction (XRD), and atomic force microscopy (AFM). The antibacterial efficacy of the synthesized nanoparticles against both Gram-negative and Gram-positive bacteria, specifically *Escherichia coli* and *Staphylococcus aureus*, was assessed by the well-diffusion technique. Following the confirmation of the antibacterial activity of the synthesized AgNPs using the well diffusion method, the minimum inhibitory concentration (MIC 50) was

obtained. Therefore, the main objective of this work is to investigate *T. orientalis* (MLETO) methanolic leaf extract as a reducing and stabilizing agent for the synthesis of AgNPs

2. Materials and methods

2.1. Collection of botanical specimens

The fresh leaves of *T. orientalis* (L.) were collected from Banaras Hindu University in Varanasi, India. The leaves were separated from the stem and rinsed extensively with double-distilled water to eliminate any impurities. The leaves were subsequently dried in the shade and then finely cut using a knife. The shredded leaves were pulverized using mechanical grinders, and the resulting powder was stored in an airtight bag for future use.

2.2. Preparation of plant extract

The methanolic leaf extract of *T. orientalis* (MLETO) was prepared by the previously method described (*39, 40*). To determine the existence of several phytochemical components in MLETO the model Orbitrap Eclipse Tribrid Mass Spectrometer from Thermo Fischer Scientific was utilized to conduct HRMS. The Dionex Ultimate 3000 RS Series was employed as the UHPLC instrument for HR-MS analysis. Three different solvent solutions, namely A, B, and C, were utilized as a mobile phase. Solvent A is composed of 100% water with 0.1% formic acid, solvent B is composed of 100% acetonitrile with 0.1% formic acid, and solvent C is composed of 100% methanol with 0.1% formic acid. The rate of flow is 0.300 mL per minute. The flow rates of sheath gas, auxiliary gas, and sweep gas are 50, 10, and 1 arbitrary unit, respectively. The duration of the run was 12 minutes. The ion source employed was heated electrospray ionization (H-ESI).

2.3. Synthesis of AgNPs

The synthesis of AgNPs was achieved through the photoinduced method. Firstly, we prepared 5 mg/mL solution by adding 50 mg of methanolic leaf extract in 1 mL of distilled water in Eppendorf tube. Mix it well. The remaining 9 mL of distilled water was added to get the desired concentration of 5 mg/mL. In the next step, 100 mL of 1 mM $AgNO_3$ (16.987 mg ~17 mg) was prepared in distilled water. $AgNO_3$ was obtained from Qualigens. To this, 5 mL of methanolic leaf extract (5 mg/mL) was added. The solution was exposed to sunlight for 3 minutes. After being exposed to daylight, the reaction mixture's color changed to dark brown from pale yellow. Upon reaction completion, centrifugation was performed for 10 minutes at 12,000 rpm. To eliminate the contaminants associated with AgNPs, the pellets were rinsed with deionized water about 2–4 times, after which the nanoparticles were vacuum-dried and preserved for subsequent use.

2.4. Characterizations of synthesized AgNPs

The change in color of the reaction mixture provided preliminary information on AgNPs green synthesis, which was validated by the absorbance of the mixture recorded by an Agilent Cary UV-Vis (ultraviolet–visible) spectrophotometer. FTIR spectroscopy was performed on powder samples of methanolic leaf extract of *T. orientalis* and AgNPs using Nicolet iS5, THERMO Electron Scientific Instruments LLC, to evaluate the presence of functional groups that are participating in the reduction and encapsulation of Ag^+ ions during the synthesis of AgNPs. An X-ray diffractometer (Rigaku Miniflex 600) coupled with a radiation source called Cu Kα and Ni filter in the range between 30–90° was used to determine the XRD pattern at 2° min^{-1} scanning rate. OriginPro 2023 was employed to determine the crystallinity index of the AgNPs. Transmission electron microscopy (TEM) was conducted through Technai 20G2. For sample preparation, a drop of synthesized AgNPs was put onto a copper grid that is coated with carbon and allowed to dry for 120 minutes at room temperature. A specimen holder was used onto which the sample was mounted. Image J software 1.8.0 version was used to obtain the size distribution histogram that helps us to determine the average size of AgNPs. Selected area electron diffraction (SAED) was merged with TEM to analyze the crystallinity of the nanoparticles. The topological properties of AgNPs were investigated using atomic force microscopy (NT-MDT, Hillsboro, Russia). Nova software 3.2.5 version was used to access the images of AFM in order to calculate the roughness, height, and depth of AgNPs.

2.5. Test organisms

The bacterial pathogens, Gram-positive (*Staphylococcus aureus*) and Gram-negative (*Escherichia coli*) were acquired from the Centre of Experimental Medicine and Surgery (CEMS), Institute of Medical Sciences (IMS), Banaras Hindu University, Varanasi, Uttar Pradesh, India, and maintained on nutrient agar.

2.6. Antibacterial assay (well diffusion method)

The antibacterial activity of methanolic leaf extracts, biosynthesized AgNPs, and commercially available

streptomycin (positive control) was compared against Gram-positive (*Staphylococcus aureus*) and Gram-negative (*Escherichia coli*) bacteria using the agar-well diffusion technique. Streptomycin was used as a positive control, while distilled water served as a negative control. The bacteria were dispersed using Mueller-Hinton agar (MHA) plates. Following the spreading process, wells were created on each plate using a well borer with a diameter of 10 mm. Different amounts of methanolic leaf extract, silver nanoparticles (AgNPs), and positive control were added to the wells. The experiment utilized positive controls, methanolic leaf extract, and AgNPs at doses of 25ug/mL, 50ug/mL, 75ug/mL, and 100ug/mL. The experiment utilized the following concentrations of Streptomycin: 25ug/mL, 50ug/mL, 75ug/mL, and 100ug/mL, which served as the positive control. The plates were placed in an incubator and kept at a temperature of 37°C for 24 hours. After the incubation period, the zone of inhibition was visualized.

2.7. Minimum inhibitory concentration (MIC50) determination

The process is based on the growth of microorganisms in suspension with variable AgNP concentrations, performed by Shanmugam and associates (*41*). In LB broth, the bacteria were cultivated for 24 hours under aerobic conditions at 37 °C. The cell count was achieved using a hemocytometer, and a standard suspension of cells (1×105 cells/mL) was obtained. The cell suspension in the concentration of 100 µL, including the control, was introduced in triplicate in the microtiter wells. Excluding the control, a 100 µL suspension of various AgNP concentrations was added to these. Wells lacking AgNPs were used as control. The inoculation wells and control were incubated for 24 hours at room temperature. The different concentrations of AgNPs utilized were as follows, 0.37, 0.78, 1.56, 3.12, 6.24, 12.5, 25, 50, and 100 µg/mL. The following day, absorbance was measured at 600 nm with a UV-visible spectrophotometer.

2.8. Statistical analysis

The groups were compared using Tukey's and Student's t-tests, and the differences between the groups were assessed using a one-way ANOVA. Test results were represented by the mean standard error of the three replicated assay-specific mean values. For each result that was achieved, the means of three replications were calculated along with the standard deviation (mean ± SD). Microsoft Excel 2016 program was used to perform statistical analysis on the data obtained. Analysis of variance (ANOVA) was used to compare the mean differences between the treatments at $p < 0.05$.

3. Results and discussion

3.1. Phytochemical analysis of methanolic leaf extract using HR-MS

The phytoconstituents were identified based on retention time, M/Z ratio, and negative and positive ion modes. HR-MS study of the MLETO identified the presence of a total of 954 compounds. The HR-MS analysis indicated the presence of the following classes of phytoconstituents in the methanolic leaf extract, flavonoids, phenolics, terpenoids, and alkaloids.

3.2. Green synthesis and UV-Vis spectroscopy analysis of AgNPs

The reducing feature of the *T. orientalis* extract was exploited and used for synthesizing AgNPs using silver nitrate as a precursor. It has been observed that *T. orientalis* possesses phytochemicals such as tremetol, quercetin, myricetin, and amentoflavone that can act as reducing agents due to its potential to donate electrons, the phenolic group improves the transformation of silver nitrate into AgNps. Several published reports have been confirmed this hypothesis on reducing different metal ions, including Zn^{2+}, Cu^{2+}, Fe^{3+}, Ti^{4+}, and Se^{2+}, using plant extracts (*42*). The shift in color to dark brown from pale yellow shows the involvement of a redox event in which the phytoconstituents of the plant reduced silver ions to silver nanoparticles. The color shift caused by sunlight is mediated by the oscillation of all free electrons in nanoparticles, a process known as surface plasmon resonance (SPR) with AgNPs (*43*). UV – Vis spectrophotometer was employed to study the reduction of Ag^{+} ions to Ag̊ by MLETO. A nanoparticle's electron cloud can oscillate on its surface, absorbing electromagnetic waves at a specific frequency as a result of the SPR phenomenon and being detected as electromagnetic wavelengths by a UV-Vis spectrophotometer (*44*). The absorbance was recorded in the range of 200–800 nm. Because of the presence of polyphenols, the UV-Vis spectra of the methanolic leaf extract revealed a strong absorption peak at 270 nm and 330 nm. Green synthesis relies on them to play a crucial part in the generation of AgNPs (*45*). The absorbance within the wavelength range of 400–500 nm is indicative of the green synthesis of AgNP, as shown in Figure 1A. The band gap energy is 2.253 eV which indicates that green synthesized nanoparticles can be used for optoelectronic and sensor development (Figure 1B).

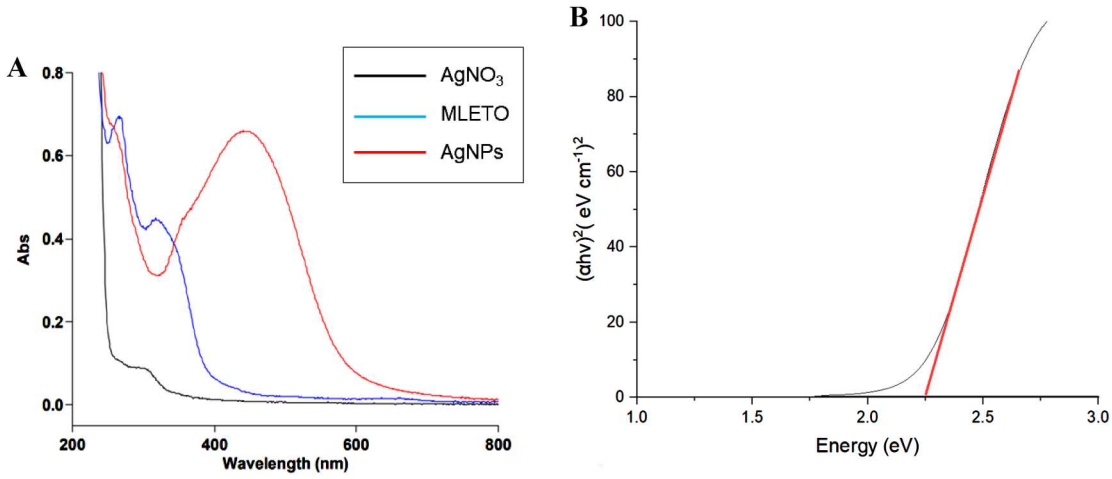

Figure 1. A) The absorbance between 400–500 nm suggests the green synthesis of silver nanoparticles (AgNPs) and B) band gap energy green synthesis of silver nanoparticles.

In comparison to other studies, where AgNPs were synthesized using *Aloe barbadensis* extract, an absorption maximum was observed at 439 nm (*46*), Similarly, AgNPs synthesized with *Thymus vulgaris* extract displayed optical properties characteristic of silver nanoparticles, with an absorption maximum within 450 nm range (*47*).

3.3. FTIR spectra analysis

The FT-IR spectroscopy is conducted to identify the likely functional groups in the plant extract responsible for capping, which leads to the enhanced stability of AgNPs (*48*). The FTIR spectra of both MLETO and AgNPs were collected in the 4000-400 cm^{-1} area, which corresponds to the stretching vibration of various functional groups. The FTIR spectra of MLETO exhibit peaks at specific wavenumbers, namely 668.2, 781, 1074, 1383, 1620, 2850, 2928, 2952, and 3428 cm^{-1}. The peaks in the FTIR spectra of AgNPs were seen at the following wavenumbers: 719.3, 833.6, 1052, 1382, 1649, 2850, 2921, 2959, and 3397 cm^{-1} (Figure 2). The peaks correspond to distinct functional groupings, as illustrated in Table 1. The signal observed at 1052 cm^{-1} corresponds to C–O stretching, which specifically indicates the presence of aliphatic alcohols. The signal observed at 1382 cm^{-1} corresponds to the C–H bending group, which is indicative of aliphatic and aromatic compounds. The peak observed at 1649 cm^{-1} corresponds to C = C bond, which is characteristic of alkenes. In addition, a clear and sharp peak observed at 1670 cm^{-1}, clearly corresponds to the presence of aldehydes or ketones compounds. The peaks at 2850, 2921, and 2959 correspond to C–H stretching group, which is indicative of aliphatic compounds. The peak observed at 3397 cm^{-1} corresponds to O-H bond, which is characteristic of phenol, hydroxy, and carboxylic acids compounds. AgNPs mediated by Cestrum

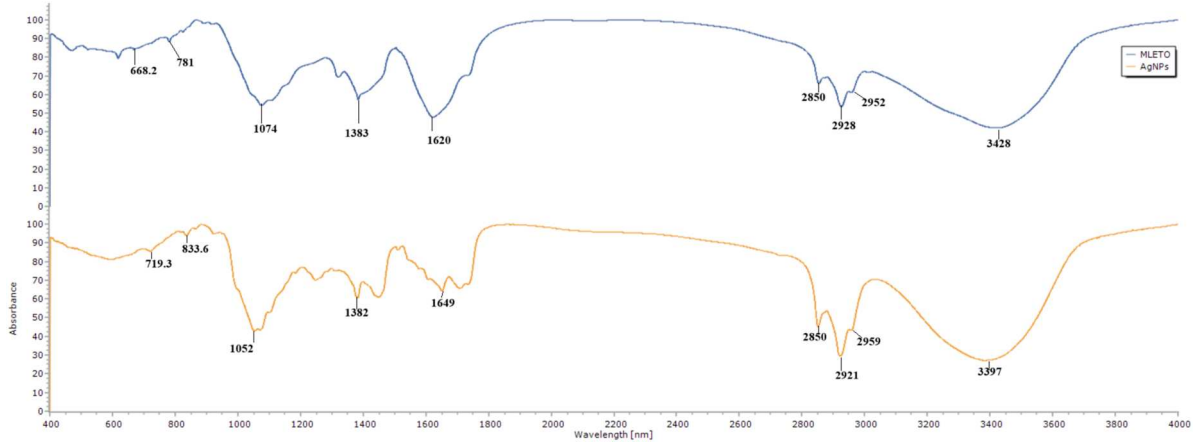

Figure 2. FTIR spectra of methanolic leaf extract of *Trema orientalis* and AgNPs.

Table 1. FTIR profiling of MLETO and AgNPs.

Frequency (cm-1)	Peak wavenumber of MLETO	Peak wavenumber of AgNPs	Functional group/Type of bond	Compounds
3550–3200	3428	3397	O-H stretching (Broad Peak)	Phenol, hydroxy, and carboxylic acid compound
3000–2800	2952	2959	C-H stretching	Aliphatic and aromatic compounds
	2928	2921		
	2850	2850		
1680–1600	1620	1649	C = C stretching	Aliphatic Alkenes
1700–1550	1670	1580	C = O stretching (sharp peak)	Carbonyl compounds
1450–1300	1320	1430	C-H bending	Aliphatic and aromatic compounds

nocturnum L. showed comparable outcomes, as stated in a previous study (*49*). Based on the aforementioned findings, it can be inferred that the peaks at 719.3, 833.6, 1070, 1649, and 3397 correspond to the flavonoid group (*50, 51*). This suggests that the primary plant compound, flavonoid, found in MLETO, has a role in the creation and durability of green AgNPs.

3.4. XRD analysis

XRD was performed to determine the crystallinity of AgNPs. AgNPs are mostly employed in powdered form for crystallinity analysis of biogenic AgNPs (*52*). The XRD pattern of AgNPs showed distinct peaks at 38.23°, 44.54°, 64.48°, 77.41°, and 81.61°, corresponding to the (111), (200), (220), (311), and (222) Bragg reflections, respectively. These results are consistent with the data provided in the JCPDS file no. 00-004-0783 (Figure 3). These reflections align with the crystallographic planes of metallic silver's face-centered cubic (fcc) crystal structure. The presence of these peaks suggests that silver plays a substantial role in the green synthesis of AgNPs. The XRD data of AgNPs synthesized from *Cestrum nocturnum* plant leaf extract showed similar results (*48*). The crystallinity index of the AgNPs is 79.28%.

3.5. TEM analysis

The shape, size, and morphology of green AgNPs are commonly studied using transmission electron microscopy (TEM) (*53*). It is observed that AgNPs are mostly in spherical shape. The size of the AgNPs ranges from 14.04–34.38 nm (Figure 4). With a decrease in the particle size of AgNPs, the surface area-to-volume ratio increases. AgNPs with sizes ranging from 10 to 100 nm display good antibacterial activity (*54*). The crystallinity of the AgNPs is confirmed by selected area electron diffraction analysis (SAED) (*55*). SAED technique is used in TEM to determine the lattice parameters, crystal structure, and degree of crystallinity of nanoparticles, using a parallel beam of electrons having high energy to target the sample (*56*). The SAED pattern and results from the XRD are in strong agreement, suggesting that AgNPs are polycrystalline as evidenced by the numerous bright concentric rings (Figure 5A). The average size of AgNPs recorded was 26.81 nm, confirmed by the size distribution histogram (Figure 5B). Energy dispersive X-ray (EDX) analysis showed the percentage relative composition of elements. The composition of elements and chemistry of the substance can be characterized using the analytical technique known as EDX. It frequently works in tandem with a TEM and a SEM. By irradiating the sample with an electron beam of high energy, the substance is subjected to the analytical process. X-rays are ejected from the atoms on the substance's surface as a result of electron bombardment (*57*). In our study, the composition of the following elements was recorded: carbon (C) 84.10%, oxygen (O) 06.20%, and silver (Ag) 11.70% (Figure 5C).

3.6. AFM analysis

Atomic force microscopy was used to analyze the topographical properties of AgNPs. The 2D photos (Figure 6A and B) and 3D images (Figure 6C and D) clearly demonstrated the spherical shape of the AgNPs, which is consistent with the results obtained from TEM analysis. The surface texture of AgNPs was highly evident. The Nova software was utilized to do image analysis on AgNPs, which involved calculating the average roughness, maximum profile peak height, and valley depth. The mean surface roughness of AgNPs was measured to be 12.054 nm. In the 2D image (Figure 6A and B), the highest height of the profile peak was 61.192 nm and the depth of the valleys was 42.719 nm. In the 3D image (Figure 6C and D), the average roughness of AgNPs was measured to be 19.489 nm. Additionally, the maximum profile peak height was found to be 189.260 nm, while the valley depth was reported as 109.856 nm.

3.7. Antibacterial assay (well diffusion method)

The agar-well diffusion technique was employed to assess the antibacterial activity of the biosynthesized AgNPs, against Gram-positive (*Staphylococcus aureus*)

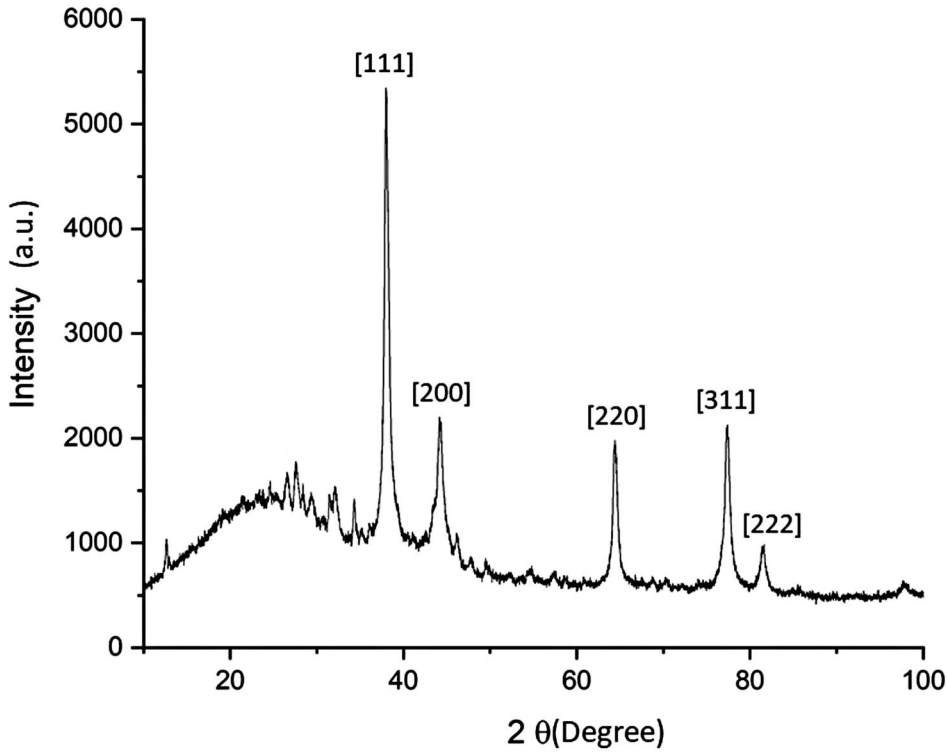

Figure 3. The XRD pattern of green synthesized AgNPs showed the diffraction peaks at 2⊖ angles of 38.23°, 44.54°, 64.48°, 77.41°, and 81.61°, which are attributed to (111), (200), (220), (311), and (222) Bragg reflections, respectively.

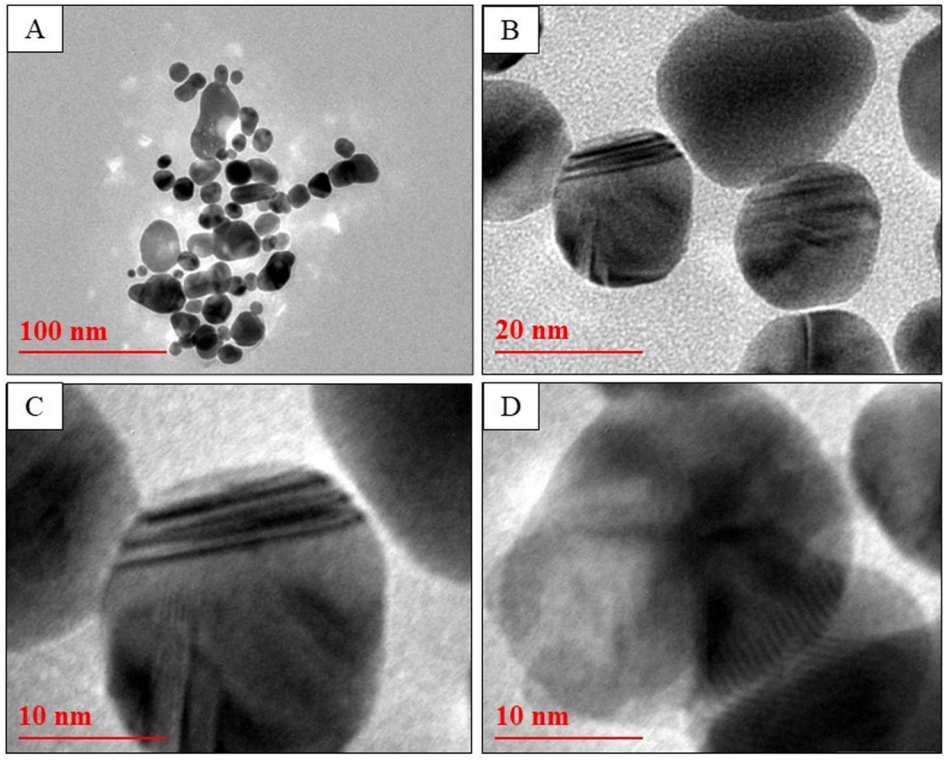

Figure 4. TEM images of green AgNPs. **(A)** TEM images of green AgNPs at 100 nm. **(B)** TEM image at 20 nm **(C)** and **(D)** TEM images at 10 nm.

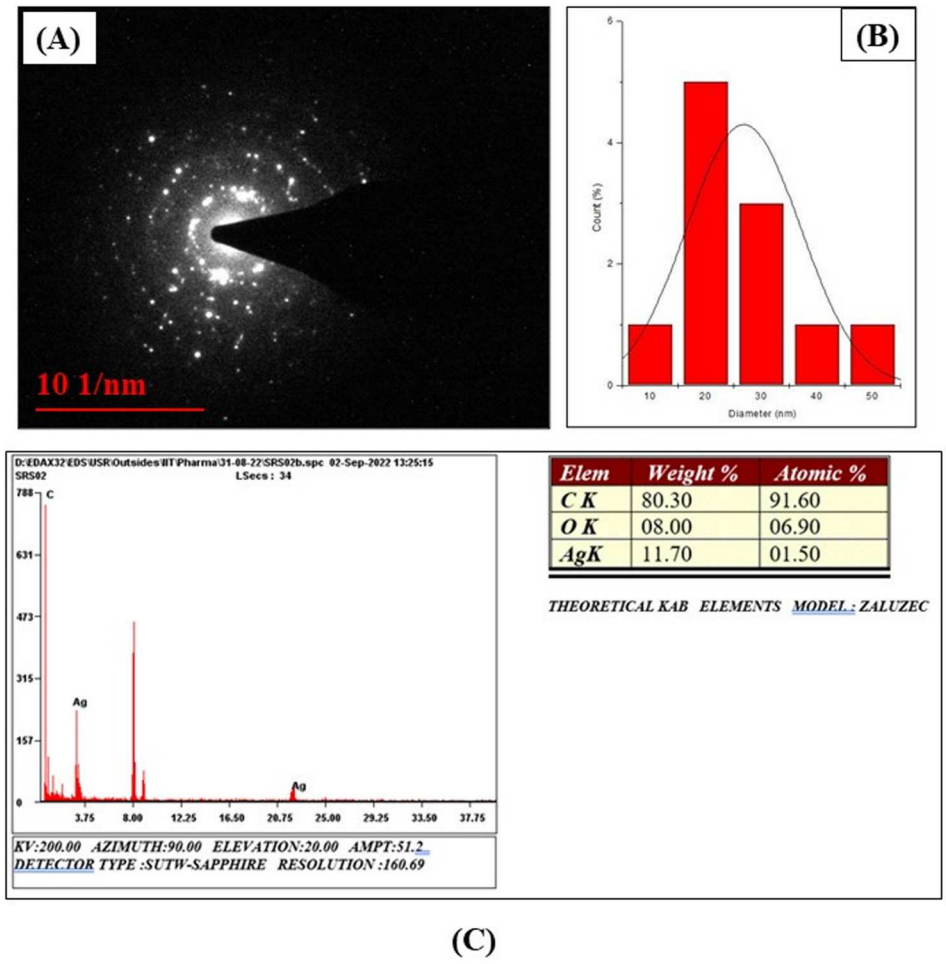

Figure 5. **(A)** SAED patterns of green AgNPs. **(B)** Size distribution histogram of green AgNPs. **(C)** EDX spectrum of green synthesized AgNP.

and Gram-negative (*Escherichia coli*). No inhibitory activity was recorded for *E. coli* (Figure 7A and Table 2) at 25 µg/mL, 50 µg/mL, 75 µg/mL, and 100 µg/mL of AgNPs. However, for *S. aureus* inhibitory activity was recorded at different concentrations of AgNPs used. At a concentration of 25 µg/mL, the zone of inhibition recorded was 9 mm. Likewise, for concentrations at 50 µg/mL, 75 µg/mL, and 100 µg/mL of AgNPs, the zone of inhibitions recorded were 10 mm, 13 mm, and 14 mm respectively (Figure 7B and Table 2). It means that zone of inhibition increases with increasing concentration AgNPs. The action mechanism of AgNPs is a result of numerous effects. It is widely acknowledged that nanoparticles have a large surface area that either permeates through the cell or adheres to the cell wall (*58*), disrupting the permeability of the membrane and making it leaky (*59*), which causes the further release of cell content. Additionally, the development of membrane pores causes nanoparticles to diffuse into the cell where they bond with proteins that contain phosphorus and sulfur, therefore, inactivating DNA and proteins (*60, 61*). The oxidation dissolution process, which releases Ag + ions, also contributes to the antibacterial action. The main interaction between the oxidized silver ions from AgNPs and the thiol groups of different enzymes and proteins is what interferes with the respiratory chain and damages the cell wall. Additionally, silver ions promote the formation of reactive oxygen species (ROS), which is thought to be the primary factor in the majority of cell deaths by inhibiting replication and ATP synthesis (*62*). The bacteria were not inhibited by the crude methanolic leaf extract in our investigation. A summary of antibacterial activity is depicted in Table 2.

3.8. Minimum inhibitory concentration (MIC50) determination

Following the confirmation of the antibacterial activity of the synthesized AgNPs using the well diffusion method in *S. aureus*, the minimum inhibitory concentration (MIC) of the AgNPs was measured. MIC is the

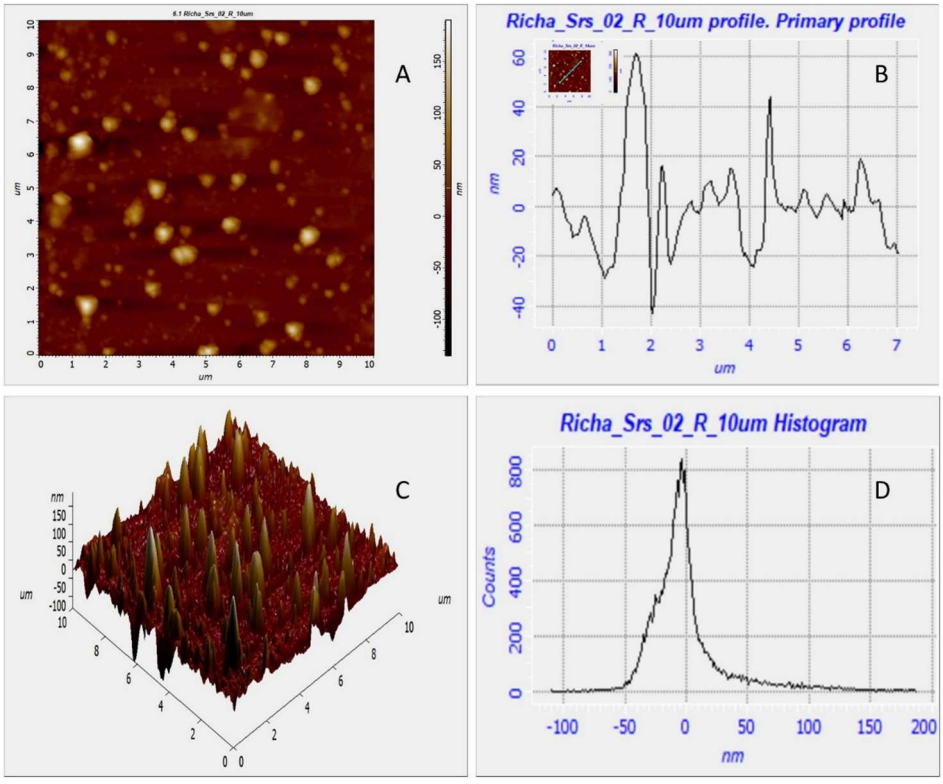

Figure 6. **(A)** Two-dimensional (2D) image of green AgNPs, **(B)** 2D roughness profile of green AgNPs, **(C)** 3D image of green AgNPs, **(D)** 3D roughness profile of green AgNPs.

lowest concentration of an antimicrobial drug that prevents the growth of bacteria (*63*, *64*). The MIC measured in S. aureus is 55.318 µg/mL.

For MIC, serial dilutions of a solution are used to find the lowest concentration of material that would still exhibit antibacterial qualities. A valid MIC assessment significantly impacts the choice of therapeutic approach, which influences the effectiveness of an infection therapy. Recent studies have focused on MIC assessment of Ag NPs against pathogenic bacteria. Recent work conducted by Ba Long Do et al, (*65*) demonstrated that MIC for silver nanoparticles is in concentrations of 8.27 µg/mL, against S. aureus. Another recent study by Imath et al. (*66*) showed that Ag-NPs efficiently inhibited Staphylococcus aureus and Escherichia coli at 100 µg/mL, with maximum inhibition zones of 15 mm and 17 mm, respectively.

4. Conclusions

The synthesis of AgNPs was achieved through the photoinduced method. UV-vis spectroscopy confirmed the green synthesis of AgNPs with the help of an absorbance peak recorded at 400 and 500 nm. Possible phytoconstituents in the leaf extract to reduce Ag + ions to Ag^{o} are identified from the FTIR spectrum. Flavonoids are the key phytoconstituents that are involved in the synthesis and stability of green AgNPs. XRD determined the crystallinity of the AgNPs, which is, 79.28%. TEM indicated that the nanoparticles had a size ranging from 14.04–34.38 nm and exhibited a spherical morphology. The majority of the AgNPs seen had an average size of 26.81 nm. The AFM was used to analyze the topographical characteristics of AgNPs that were synthesized using a green method. The Nova software was utilized to do image analysis on AgNPs, which involved calculating the average roughness, maximum profile peak height, and valley depth. The mean surface roughness of AgNPs was measured to be 12.054 nm. In the 2D image, the highest point of the profile reached a height of 61.192 nm, while the valleys had a depth of 42.719 nm. The 3D image revealed that the average roughness of AgNPs was 19.489 nm. Additionally, the maximum height of the profile peak was recorded as 189.260 nm, while the depth of the valley was measured at 109.856 nm. The synthesized nanoparticles exhibited antibacterial activity against *S. aureus*, as determined by the agar well diffusion method. The zone of inhibition measured 9, 10, 13, and 14 mm at concentrations of 25, 50, 75, and 100 µg/mL, respectively. The minimum inhibitory concentration (MIC50) recorded against *S. aureus* is 55.31 µg/ml. Our research is significant as a

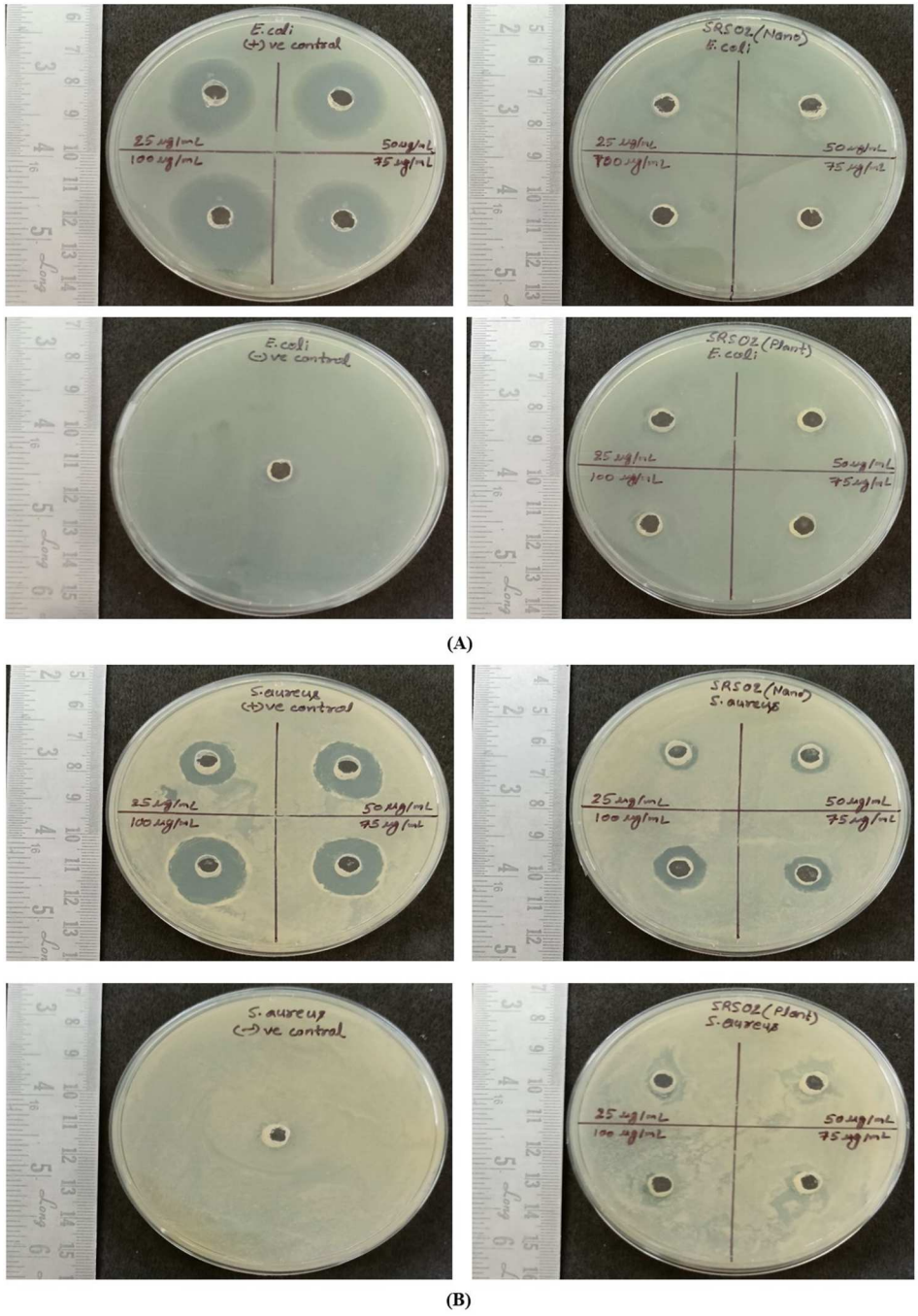

Figure 7. Antibacterial activity against **(A)** *E. coli* and **(B)** *S. Aureus*.

Table 2. Antimicrobial activity of Trema orientalis against S. aureus.

Bacteria	Concentration of AgNPs (µg/mL)	Diameter of zone of inhibition (mm)
Escherichia coli	25	0
	50	0
	75	0
	100	0
Staphylococcus aureus	25	9
	50	10
	75	13
	100	14

first finding that suggests that silver nanoparticles made from *Trema orientalis* leaf extract have the potential to be used as an antimicrobial agent. Further testing of the antimicrobial activity of AgNPs in different microorganisms can yield more useful results.

Acknowledgments

The authors would like to acknowledge Deanship of Graduate Studies and Scientific Research, Taif University for funding this work. VDR acknowledge the support by the Strategic Academic

Leadership Program of the Southern Federal University ("Priority 2030").

Author contributions

'Conceptualization, R.D. and P.K.; methodology, RD.; software, Sh.A.; validation, S.A., F.A.A and A.K.AA.; formal analysis, A.K.S.; investigation, I.B.; resources, K.N.T.; data curation, S.K.M.and I.B.; writing – original draft preparation, A.K.T.; writing – review and editing, W.J.A, V.D.R, and Z.T.A.; visualization, P.K. and Z.T.A.; supervision, S.K.M. and S.A. project administration, S.K.M.; funding acquisition, P.K. All authors have read and agreed to the published version of the manuscript.'

Disclosure statement

No potential conflict of interest was reported by the author(s).

ORCID

Zaidon T. Al-aqbi http://orcid.org/0000-0002-9578-4228

References

[1] Jeevanandam, J.; Barhoum, A.; Chan, Y.S.; Dufresne, A.; Danquah, M.K. Review on Nanoparticles and Nanostructured Materials: History, Sources, Toxicity and Regulations. *Beilstein J. Nanotechnol* **2018,** *9*, 1050–1074.

[2] Ragavendran, C.; Kamaraj, C.; Jothimani, K.; Priyadharsan, A.; Kumar, D.A.; Natarajan, D.; Malafaia, G. Eco-friendly Approach for ZnO Nanoparticles Synthesis and Evaluation of its Possible Antimicrobial, Larvicidal and Photocatalytic Applications. *Sustain Mater Technol* **2023**, *36*, e00597. doi:10.1016/j.susmat.2023.e00597.

[3] Rokkarukala, S.; Cherian, T.; Ragavendran, C.; Mohanraju, R.; Kamaraj, C.; Almoshari, Y.; Albariqi, A.; Sultan, M.H.; Alsalhi, A.; Mohan, S. One-pot Green Synthesis of Gold Nanoparticles Using *Sarcophyton Crassocaule*, a Marine Soft Coral: Assessing Biological Potentialities of Antibacterial, Antioxidant, Anti-Diabetic and Catalytic Degradation of Toxic Organic Pollutants. *Heliyon* **2023**. doi:10.1016/j.heliyon.2023.e14668.

[4] Sivakumar, S.; Subban, M.; Chinnasamy, R.; Chinnaperumal, K.; Nakouti, I.; El-Sheikh, M.A.; Shaik, J.P. Green Synthesized Silver Nanoparticles Using *Andrographis Macrobotrys* Nees Leaf Extract and its Potential to Antibacterial, Antioxidant, Anti-Inflammatory and Lung Cancer Cells Cytotoxicity Effects. *Inorg. Chem. Commun* **2023**, *153*, 110787.

[5] Messaoudi, O.; Benamar, I.; Azizi, A.; Albukhaty, S.; Khane, Y.; Sulaiman, G.M.; Salem-Bekhit, M.M.; Hamdi, K.; Ghoummid, S.; Zoukel, A.; Messahli, I. Characterization of Silver Carbonate Nanoparticles Biosynthesized Using Marine *Actinobacteria* and Exploring of Their Antimicrobial and Antibiofilm Activity. *Mar. Drugs* **2023,** *21*, 536. doi:10.3390/md21100536.

[6] Alamier, W.M.; Hasan, N.; Ali, S.K.; Oteef, M.D.Y. Green Synthesis of Ag Nanoparticles Using *Caralluma Acutangula* Extract and Its Catalytic Functionality Towards Degradation of Hazardous Dye Pollutants. *Crystals. (Basel)* **2022,** *12*, 1069. doi:10.3390/cryst12081069.

[7] Ragavendran, C.; Kamaraj, C.; Natarajan, D.; Al-Ghanim, K.A.; Magesh, M.; Nicoletti, M.; Govindarajan, M. Synthesis of *Lawsonia Inermis*-Encased Silver–Copper Bimetallic Nanoparticles with Antioxidant, Antibacterial, and Cytotoxic Activity. *Green Process. Synth* **2024,** *13* (1), 20230194. doi:10.1515/gps-2023-0194.

[8] Khan, I.; Saeed, K.; Khan, I. Nanoparticles: Properties, Applications and Toxicities. *Arab. J. Chem* **2019**, *12*, 908–931.

[9] Ali, F.; Ali, A.; Din, G.M.U.; Younas, U.; Nazir, A.; Akyürekli, S.; Iqbal, M.; Mnif, W.; Algarni, Z. Silver and Zinc Oxide Decorated rGO Nanocomposites as Efficient Electrocatalysts Towards Oxygen Evolution Reactions Under Alkaline Conditions. *Diamond Relat. Mater.* **2024,** *148*, 111378.

[10] Safat, S.; Buazar, F.; Albukhaty, S.; Matroodi, S. Enhanced Sunlight Photocatalytic Activity and Biosafety of Marine-Driven Synthesized Cerium Oxide Nanoparticles. *Sci. Rep.* **2021,** *11*, 14734. doi:10.1038/s41598-021-94327-w.

[11] Shoukat, J.; Abd-Ur-Rahman, H.M.; Muhammad, A.J.; Obaid, S.; Imtiaz, F.; Kanwal, N.; Mnif, W.; Ali, A.; Nazir, A.; Ahmad, N.; Iqbal, M. The Interaction Between Formylphenoxyacetic Acid Derivatives (Chalcone and Flavones) and Ionic Surfactants: Insights Into Binding Constants, Solubilisation and Physiochemical Properties. *Colloids Surf., B* **2024,** *240*, 113976.

[12] Hussain, S.; Zahid, A.; Imran, M.; Massey, S.; Riaz, M.; Sagir, M.; Shahid, M.; Mnif, W.; Iqbal, S.; Iqbal, M.; Nazir, A. Unveiling the Chemical Profile, Synergistic Antibacterial and Hemolytic Effects of Cymbopogon Citratus and Tachyspermum Ammi Leaves. *Biocatal. Agric. Biotechnol* **2024,** *58*, 103221.

[13] Neamah, S.A.; Albukhaty, S.; Falih, I.Q.; Dewir, Y.H.; Mahood, H.B. Green Synthesis of Zinc Oxide Nanoparticles Using *Capparis Spinosa* L. Fruit Extract: Characterization, Biocompatibility, and Antioxidant Activity. *Appl. Sci* **2023,** *13* (11), 6604. doi:10.3390/app13116604.

[14] Urnukhsaikhan, E.; Bold, B.E.; Gunbileg, A.; Sukhbaatar, N.; Mishig-Ochir, T. Antibacterial Activity and Characteristics of Silver Nanoparticles Biosynthesized from *Carduus Crispus*. *Sci. Rep* **2021,** *26*, 21047.

[15] Nazir, A.; Abbas, M.; Kainat, F.; Iqbal, D.N.; Aslam, F.; Kamal, A.; Mohammed, O.A.; Zafar, K.; Alrashidi, A.A.; Alshawwa, S.Z.; Iqbal, M. Efficient Drug Delivery Potential and Antimicrobial Activity of Biocompatible Hydrogels of Dextrin/Na-Alginate/PVA. *Heliyon* **2024,** *10* (9.

[16] Jamkhande, P.G.; Ghule, N.W.; Bamer, A.H.; Kalaskar, M.G. Metal Nanoparticles Synthesis: An Overview on Methods of Preparation, Advantages and Disadvantages, and Applications. *J. Drug Deliv. Sci. Technol* **2019,** *53*, 101174.

[17] Khane, Y.; Benouis, K.; Albukhaty, S.; Sulaiman, G.M.; Abomughaid, M.M.; Al Ali, A.; Aouf, D.; Fenniche, F.; Khane, S.; Chaibi, W.; Henni, A. Green Synthesis of Silver Nanoparticles Using Aqueous *Citrus Limon* Zest Extract: Characterization and Evaluation of Their Antioxidant

and Antimicrobial Properties. *Nanomaterials* **2022,** *12*, 2013. doi:10.3390/nano12122013.

[18] Iqbal, J.; Abbasi, B.H.; Mahmood, T.; Kanwal, S.; Ali, B.; Shah, S.A.; Khalil, A.T. Plant-derived Anticancer Agents: A Green Anticancer Approach. *Asian Pac. J. Trop. Biomed* **2017,** *7*, 1129–1150.

[19] Saleem, A.; Iqbal, A.; Younas, U.; Ashraf, A.; Al-Mijalli, S.H.; Ali, F.; Pervaiz, M.; Saeed, Z.; Nazir, A.; Iqbal, M. Antimicrobial Attributes and Enhanced Catalytic Potential of PVA Stabilized Ag-NiO2 Nanocomposite for Wastewater Treatment. *Arabian J. Chem* **2024,** *17* (2), 105545.

[20] Xu, D.P.; Li, Y.; Meng, X.; Zhou, T.; Zhou, Y.; Zheng, J.; Zhang, J.J.; Li, H.B. Natural Antioxidants in Foods and Medicinal Plants: Extraction, Assessment and Resources. *Int. J. Mol. Sci.* **2017,** *18* (1), 96.

[21] Banala, R.R.; Nagati, V.B.; Karnati, P.R. Green Synthesis and Characterization of Carica Papaya Leaf Extract Coated Silver Nanoparticles Through X-ray Diffraction, Electron Microscopy and Evaluation of Bactericidal Properties. *Saudi J. Biol. Sci.* **2015,** *22* (5), 637–644.

[22] Sathishkumar, M.; Sneha, K.; Won, S.W.; Cho, C.W.; Kim, S.; Yun, Y.S. Cinnamon Zeylanicum Bark Extract and Powder Mediated Green Synthesis of Nano-Crystalline Silver Particles and its Bactericidal Activity. *Colloids Surf., B* **2009**, *73* (2), 332–338.

[23] Imtiaz, F.; Saif, Z.; Sajid, A.; Nazir, A.; Manzoor, Q.; Saleem, A.; Farooq, A.; Al-Mijalli, S.H.; Iqbal, M. Role of Glycerol-Based Deep Eutectic Solvents for Extraction of Phytochemicals from Cichorium Intybus Seeds: Optimization by Response Surface Methodology. *Microchem. J.* **2024,** *199*, 110083.

[24] Gomathi, M.; Rajkumar, P.V.; Prakasam, A.; Ravichandran, K. Green Synthesis of Silver Nanoparticles Using Datura Stramonium Leaf Extract and Assessment of Their Antibacterial Activity. *Resour-Effic. Technol* **2017,** *3* (3), 280–284.

[25] Saha, J.; Begum, A.; Mukherjee, A.; Kumar, S. A Novel Green Synthesis of Silver Nanoparticles and Their Catalytic Action in Reduction of Methylene Blue dye. *Sustainable Environ. Res* **2017**, *27* (5), 245–250.

[26] Jyoti, K.; Baunthiyal, M.; Singh, A. Characterization of Silver Nanoparticles Synthesized Using Urtica Dioica Linn. Leaves and Their Synergistic Effects with Antibiotics. *J Radiat. Res. Appl. Sci* **2016,** *9* (3), 217–227.

[27] Jung, W.K.; Koo, H.C.; Kim, K.W.; Shin, S.; Kim, S.H.; Park, Y.H. Antibacterial Activity and Mechanism of Action of the Silver ion in Staphylococcus Aureus and Escherichia Coli. *Appl. Environ. Microbiol* **2008,** *74*, 2171–2178. doi:10.1128/AEM.02001-07.

[28] Matsumura, Y.; Yoshikata, K.; Kunisaki, S.I.; Tsuchido, T. Mode of Bactericidal Action of Silver Zeolite and its Comparison with That of Silver Nitrate. *Appl. Environ. Microbiol.* **2003,** *69* (7), 4278–4281.

[29] Feng, Q.L.; Wu, J.; Chen, G.Q.; Cui, F.Z.; Kim, T.N.; Kim, J.O. A Mechanistic Study of the Antibacterial Effect of Silver Ions on Escherichia Coli and Staphylococcus Aureus. *J. Biomed. Mater. Res.* **2000,** *52* (4), 662–668.

[30] Kim, J.S.; Kuk, E.; Yu, K.N.; Kim, J.H.; Park, S.J.; Lee, H.J.; Cho, M.H. Antimicrobial Effects of Silver Nanoparticles. *Nanomed. Nanotechnol. Biol. Med.* **2007,** *3* (1), 95–101.

[31] Adinortey, M.B.; Galyuon, I.K.; Asamoah, N.O. Trema Orientalis Linn. Blume: A Potential for Prospecting for Drugs for Various Uses. *Pharmacogn. Rev.* **2013,** *7* (13), 67.

[32] Farzana, M.; Rahman, M.M.; Ferdous, T.; Jahan, M.S. Review on Trema Orientalis as a Potential Bioresource in Tropical Countries. *Trees* **2022,** *36* (4), 1169–1177.

[33] Olanlokun, J.O.; David, O.M.; Afolayan, A.J. In Vitro Antiplasmodial Activity and Prophylactic Potentials of Extract and Fractions of Trema Orientalis (Linn.) Stem Bark. *BMC Complement. Altern. Med.* **2017**, *17* (1), 1–11.

[34] Saleh, A.; Zainal-Ariffin, S.M.; Yahaya, S.F.; Khaleel, A.G. Antioxidant Activities and Estimation of Phenol and Flavonoid Contents in the Extracts of Trema Orientalis Linn Blume. *Niger. Vet. J* **2020**, *41* (2), 73–84.

[35] Oyebola, O.E.; Morenikeji, O.A.; Ademola, I.O. In-vivo Antimalarial Activity of Aqueous Leaf and Bark Extracts of Trema Orientalis Against Plasmodium Berghei in Mice. *J. Parasit. Dis.* **2017,** *41*, 398–404.

[36] Sayeed, M.A.; Jainul, M.A.; Azam, S.; Babar, Z.M.; Azad, A.K. In Vivo Antidiarrheal Activity of Methanolic Extract of Trema Oreintalis Leaves. *Ph. OL* **2017,** *2*, 187–192.

[37] Uddin, S.N.; Yesmin, M.N.; Pramanik, M.K.; Akond, M.A. Antiinflammatory, Antinociceptive and Diuretic Activities of Trema Orientalis Linn. *Adv. Tradit. Med* **2009,** *9* (4), 320–325.

[38] Ajayi, G.O.; Idoko, A.; Usman, A. Phytochemical Analysis and Antibacterial Activity of Trema Orientalis (Ulmaceae) Stem Bark Extracts on Respiratory Tract Bacteria. *Trop. J. Nat. Prod. Res* **2018,** *2* (12), 512–516.

[39] Alzubaidi, A.K.; Al-Kaabi, W.J.; Ali, A.A.; Albukhaty, S.; Al-Karagoly, H.; Sulaiman, G.M.; Asiri, M.; Khane, Y. Green Synthesis and Characterization of Silver Nanoparticles Using Flaxseed Extract and Evaluation of Their Antibacterial and Antioxidant Activities. *Appl. Sci.* **2023,** *13* (4), 2182. doi:10.3390/app13042182.

[40] Magesh, M.; Thadanki, M.L.; Alam, M.W.; Kishore, V.; Ragavendran, C. Sustainable Synthesis of Ag-NPs from *Cassia Auriculata* Flower Extract: Synthesis, Spectral Characterization, its Biomedical and Environmental Applications. *Nanotechnol. Environ. Eng* **2024**, *9*, 161–177. doi:10.1007/s41204-024-00365-w.

[41] Shanmugam, J.; Dhayalan, M.; Savaas Umar, M.R.; Gopal, M.; Ali Khan, M.; Simal-Gandara, J.; Cid-Samamed, A. Green Synthesis of Silver Nanoparticles Using *Allium Cepa* var. *Aggregatum* Natural Extract: Antibacterial and Cytotoxic Properties. *Nanomaterials* **2022,** *12*, 1725. doi:10.3390/nano12101725.

[42] Al-aqbi, Z.T.; Abdulsahib, H.T.; Al-Doghachi, F.A. A Portable Microfluidic Device-Based Colorimetric Naked-Eye Sensors for Determination of Mercury and Arsenic Ions in River Water Samples. *Plasmonics.* **2024**, 1–22. doi:10.1007/s11468-024-02237-0.

[43] Debnath, G.; Das, P.; Saha, A.K. Green Synthesis of Silver Nanoparticles Using Mushroom Extract of Pleurotus Giganteus: Characterization, Antimicrobial, and α-Amylase Inhibitory Activity. *Bionanoscience.* **2019,** *9*, 611–619.

[44] Mat Yusuf, S.N.A.; Che Mood, C.N.A.; Ahmad, N.H.; Sandai, D.; Lee, C.K.; Lim, V. Optimization of Biogenic Synthesis of Silver Nanoparticles from Flavonoid-Rich *Clinacanthus Nutans* Leaf and Stem Aqueous Extracts. *R. Soc. Open. Sci.* **2020,** *7* (7), 200065. doi:10.1098/rsos.200065.

[45] Kumar, P.; Dixit, J.; Singh, A.K.; Rajput, V.D.; Verma, P.; Tiwari, K.N.; Mishra, S.K.; Minkina, T.; Mandzhieva, S. Efficient Catalytic Degradation of Selected Toxic Dyes by Green Biosynthesized Silver Nanoparticles Using Aqueous Leaf Extract of *Cestrum Nocturnum* L. *Nanomaterials (Basel)* **2022,** *12* (21), 3851. doi:10.3390/nano12213851.

[46] Ghatage, M.M.; Mane, P.A.; Gambhir, R.P.; Parkhe, V.S.; Kamble, P.A.; Lokhande, C.D.; Tiwari, A.P. Green Synthesis of Silver Nanoparticles via Aloe Barbadensis Miller Leaves: Anticancer, Antioxidative, Antimicrobial and Photocatalytic Properties. *Appl. Surf. Sci. Adv* **2023,** *16*, 100426. doi:10.1016/j.apsadv.2023.100426.

[47] Tavukcuoglu, O.; Duygulu, N.E.; Altinbay, A.; Ciftci, F. Green Synthesis of Silver Nanoparticles from Thymus Vulgaris and Sambucus Nigra Extracts in Poly (Vinyl Alcohol) Nanofiber Matrix: In Vitro Evaluation. *Ind. Crops Prod.* **2024**, *222*, 119825.

[48] Noh, C.H.C.; Azmin, N.F.M.; Amid, A. Principal Component Analysis Application on Flavonoids Characterization. *Adv. Sci. Technol. Eng. Syst. J* **2017,** *2*, 435–440.

[49] Heneczkowski, M.; Kopacz, M.; Nowak, D.; Kuźniar, A. Infrared Spectrum Analysis of Some Flavonoids. *Acta Pol. Pharm.* **2001,** *58* (6), 415–420.

[50] Kumar, P.; Sonkar, P.K.; Tiwari, K.N.; Singh, A.K.; Mishra, S.K.; Dixit, J.; Ganesan, V.; Singh, J. Sensing of Mercury ion Using Light Induced Aqueous Leaf Extract Mediated Green Synthesized Silver Nanoparticles of Cestrum Nocturnum L. *Environ. Sci. Pollut. Res* **2022,** *29* (53), 79995–80004.

[51] Zhang, X.F.; liu, Z.-G.; shen, W.; Gurunathan, S. Silver Nanoparticles: Synthesis, Characterization, Properties, Applications, and Therapeutic Approaches. *Int. J. Mol. Sci.* **2016,** *17*, 1534.

[52] Morones, J.R.; Elechiguerra, J.L.; Camacho, A.; Holt, K.; Kouri, J.B.; Ramírez, J.T.; Yacaman, M.J. The Bactericidal Effect of Silver Nanoparticles. *Nanotechnology* **2005,** *16* (10), 2346.

[53] Venugopal, K.; Rather, H.A.; Rajagopal, K.; Shanthi, M.P.; Sheriff, K.; Illiyas, M.; Maaza, M. Synthesis of Silver Nanoparticles (Ag NPs) for Anticancer Activities (MCF 7 Breast and A549 Lung Cell Lines) of the Crude Extract of Syzygium Aromaticum. *J. Photochem. Photobiol., B* **2017,** *167*, 282–289.

[54] Behera, A.; Pradhan, S.P.; Ahmed, F.K.; Abd-Elsalam, K.A. Enzymatic synthesis of silver nanoparticles: Mechanisms and applications. In *Green Synthesis of Silver Nanomaterials*; Elsevier; pp 699–756.

[55] Thambiratnam, K.; Reduan, S.A.; Tiu, Z.C.; Ahmad, H. Application of Two-Dimensional Materials in Fiber Laser Systems. In *Nano-Optics*; Elsevier: Amsterdam, The Netherlands, 2020; pp 227–264.

[56] Siddiqi, K.S.; Husen, A.; Rao, R.A.K. A Review on Green Synthesis of Silver Nanoparticles and Their Biocidal Properties. *J. Nanobiotechnol* **2018,** *16*, 1–28.

[57] Kambale, E.K.; Nkanga, C.I.; Mutonkole, B.P.I.; Bapolisi, A.M.; Tassa, D.O.; Liesse, J.M.I.; Krause, R.W.; Memvanga, P.B. Green Synthesis of Antimicrobial Silver Nanoparticles Using Aqueous Leaf Extracts from Three Congolese Plant Species (*Brillantaisia Patula, Crossopteryx Febrifuga and Senna Siamea*). *Heliyon* **2020**, *6*, e04493.

[58] Vijayan, R.; Joseph, S.; Mathew, B. Green Synthesis, Characterization and Applications of Noble Metal Nanoparticles Using *Myxopyrum Serratulum* A.W. Hill Leaf Extract. *Bio. Nano Sci* **2018,** *8*, 105–117.

[59] Ahmad, W.; Ahmed, S.; Kumar, S. Facile one Step Microwave Assisted Biofabrication of Fe_2O_3 NPs: Potential Application as Solar Light-Driven Photocatalyst in the Photodegradation of Acridine Orange. *Int. J. Environ. Anal. Chem.* **2024**, 1–16. doi:10.1080/03067319.2024.2344707.

[60] Liao, C.; Li, Y.; Tjong, S.C. Bactericidal and Cytotoxic Properties of Silver Nanoparticles. *Int. J. Mol. Sci* **2019**, *20*, 449. doi:10.3390/ijms20020449.

[61] Jabir, M.S.; Mohammed, M.K.; Albukhaty, S.; Ahmed, D.S.; Syed, A.; Elgorban, A.M.; Eswaramoorthy, R.; Al-kuraishy, H.M.; Al-Gareeb, A.I.; Ghotekar, S.; Jawad, S.F. Functionalized SWCNTs@Ag–TiO_2 Nanocomposites Induce ROS-Mediated Apoptosis and Autophagy in Liver Cancer Cells. *Nanotechnol. Rev.* **2003,** *12* (1), 20230127. doi:10.1515/ntrev-2023-0127.

[62] Ahmad, W.; Joshi, H.; Ahmed, S.; Kumar, S.; Wilson, I. Parmelia Perlata Mediated Microwave-Assisted one-pot Green Synthesis of NiO Nanoparticles a Noble Approach: Antibacterial and Photocatalytic Activity Evaluation. *Chem. Phys. Lett.* **2024,** *853*, 141524. doi:10.1016/j.cplett.2024.141524.

[63] Andrews, J.M. Determination of Minimum Inhibitory Concentrations. *J. Antimicrob. Chemother* **2001**, *48*, 5–16.

[64] Ahmad, W.; Ahmed, S.; Kumar, S.; Joshi, H.C. Facile one Step Microwave-Assisted Bioextract-Mediated Green Synthesis of ZnO NPs and Subsequent Investigation of Their Antibacterial and Photocatalytic Activity. *Chem. Pap* **2024**, *78*, 8309–8320. doi:10.1007/s11696-024-03669-y.

[65] Do, B.L.; Bui, T.H.; Ho, T.G.T.; Duong, N.L.; Dang-Bao, T.; Nguyen, T.; Phuong, P.H. Green Synthesis of Nano-Silver and its Antibacterial Activity Against Methicillin-Resistant Staphylococcus Aureus. *J. Saudi Chem. Soc.* **2023**, *27* (5), 101722.

[66] Imath, M.; Ragavendran, C.; Kamaraj, C.; Alrefaei, A.F.; Almutairi, M.H.; Raj, M.; Rajendran, R.; Paneerselvam, T.; Arasu, T.; Martin, T.M.; Sundaram, M. Fioria Vitifolia-Mediated Silver Nanoparticles: Eco-Friendly Synthesis and Biomedical Potential. *J. Water Process Eng* **2024**, *66*, 106020.